Design and Development of a Livox-Based Indoor Surveying System for Floor Mapping Applications

Walid Darwish[1, 2]*, Mostafa G. Abdelmageed [3], Moustafa Baraka [4], Adel ElShazly [1], Ahmad M. Senousi [1, 2], Wael Ahmed[1, 2]

[1] Public Works Department, Faculty of Engineering, Cairo University,
Giza, Egypt, 12613.(walid.darwish & wael.mohamed) @cu.edu.eg
[2] NAMAA for Engineering Consultations, Dokki , Giza, Egypt
[3] Mechanical Design & Production Department, Faculty of Engineering, Cairo University, Giza 12613, Egypt
[4] Civil Engineering Program, German University in Cairo 11835, Egypt

Keywords: LiDAR, IMU, SLAM, Camera Pose, Mapping

Abstract

Accurate three-dimensional (3D) data acquisition of indoor environments remains a challenging and resource-intensive task, particularly for fully furnished spaces. This study presents the development and implementation of a low-cost wearable surveying system for efficient 3D indoor data acquisition. The proposed system integrates a Livox Mid-360 LiDAR sensor and an RGB camera mounted on a helmet, both controlled via a mini-PC unit for synchronized data collection. The captured LiDAR frames and inertial measurement unit (IMU) data are fused with RGB imagery using a Simultaneous Localization and Mapping (SLAM) framework to generate 3D reconstruction of interior structures. The resulting point clouds and wall models are evaluated based on RANSAC line fitting method to assess their geometric accuracy and structural consistency. Moreover, a ground truth measurements were collected to verify the absolute accuracy of the resulting point clouds. The proposed approach demonstrates the potential of cost-effective, portable solutions for indoor 3D mapping and documentation with a cm-level of accuracy.

1. Introduction

Three-dimensional digital databases are essential for a wide range of applications and have long been a key focus of research in domains such as construction and entertainment. Its significance has further expanded within architecture, engineering, and construction (AEC) fields, especially with the increasing integration of Building Information Modeling (BIM) into AEC workflow (Hany et al., 2025; Mahmoud et al., 2025; Wang and Li, 2024). Various automated data acquisition methods have been extensively explored in recent years, reflecting the growing need for efficient and accurate spatial data collection. Indoor mapping, in particular, has gained significant attention due to its critical role in creating precise three-dimensional representations of built environments. Depending on the employed technology, data acquisition systems can generally be categorized as either camera-based (Wu et al., 2025) or laser-based (Mahmoud et al., 2025). Camera-based systems utilize optical sensors to capture visual information and reconstruct spatial geometry using different photogrammetric techniques. In contrast, laser-based systems rely on Light Detection and Ranging (LiDAR) technology to measure distances and generate dense point clouds with high geometric accuracy (Willkens et al., 2024). Beyond sensor typology, classification can also be made according to the deployment platform. Terrestrial mapping systems operate from stationary ground-based setups, enabling the capture of highly detailed and accurate measurements within limited spatial ranges (Sánchez-Aparicio et al. (2018); Willkens et al. (2024)). Conversely, mobile mapping systems integrate sensors on moving platforms—such as handheld devices, ground vehicles, or robotic carriers—allowing efficient large-scale data acquisition while maintaining acceptable accuracy levels (Hany et al. (2025); Wang and Li (2024); Wang et al. (2025); Xu et al. (2025); Zhao et al. (2024)). These technological advancements have substantially improved data collection workflows, supporting a wide range of applications in indoor modeling, digital twin development, and the broader domains of AEC (Hany et al., 2025).

* Corresponding author

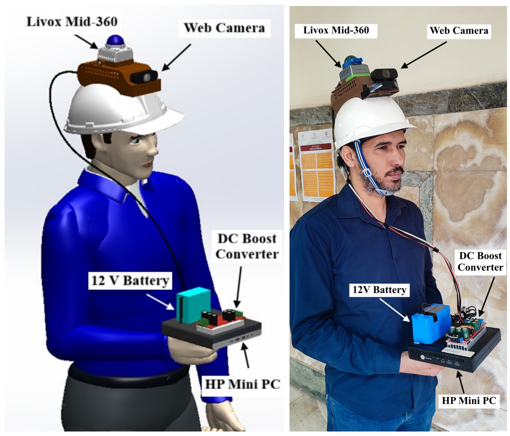

(a) System design (b) Implementation

Figure 1. Wearable Scanning Platform components from design (a) to application (b)

Recent research has highlighted significant progress in Simultaneous Localization and Mapping (SLAM) techniques, particularly in their application to compact wearable mapping systems that utilize LiDAR sensors for precise three-dimensional perception. SLAM enables a system to simultaneously determine its spatial position (localization) and construct a real-time map of previously unknown environments (mapping), making it a fundamental approach for accurate and efficient modeling of complex and unstructured environments (Li et al., 2024; Yoshida et al., 2023; Zhao et al., 2024). Zhang et al. (2025) proposed

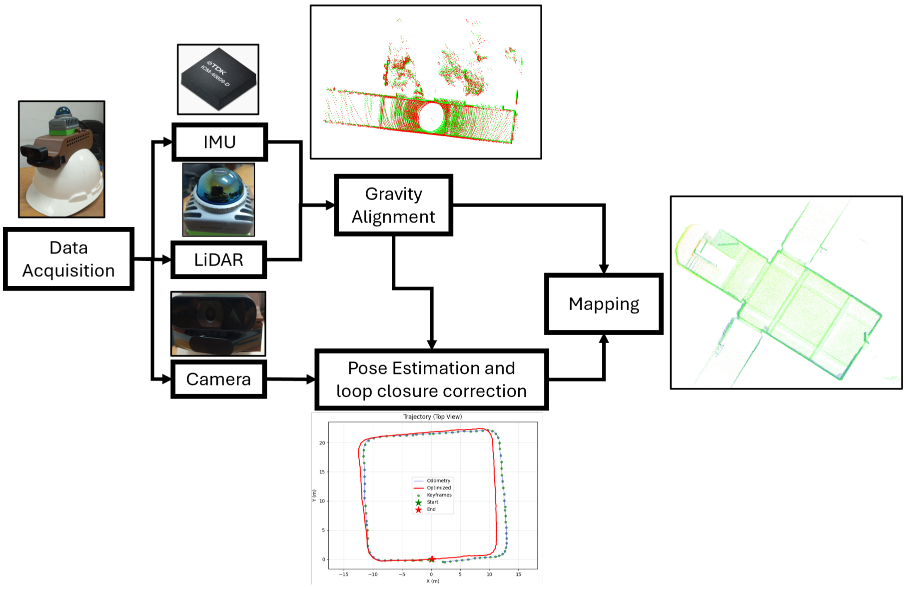

Figure 2. The proposed workflow for 3D point reconstruction

an approach for algorithm that combines LiDAR-based SLAM, total station measurements, and graph optimization to optimize the robot’s trajectory in indoor environments. Highly accurate positional data from total station measurements was adopted as additional constraints, indoor LiDAR SLAM. Wang et al. (2025) introduced a three-dimensional LiDAR SLAM framework incorporating multilayer horizontal plane optimization to enhance robustness and precision in indoor environments. The proposed system integrates a plane clustering segmentation algorithm that segments raw point clouds based on horizontal and vertical curvature, enabling simultaneous extraction of feature points and inclined planes. By combining this segmentation with feedback from LiDAR odometry, the method corrects the sensor’s tilt and improves ground plane detection under large-angle motion. Additionally, edge and surface feature matching are fused with horizontal plane optimization to refine LiDAR odometry and suppress pose drift.

Li et al. (2024) introduced a LiDAR–Inertial Odometry (LIO) framework designed for compact wearable mapping systems (WMSs), built upon a Hybrid Continuous-Time Optimization (HCTO) approach that accounts for the optimality of LiDAR correspondences. The proposed HCTO framework first analyzes raw IMU measurements to identify distinct patterns in human motion, including high-frequency, low-frequency, and constant-velocity components. Based on these motion states, hybrid IMU factors are then constructed to enable robust and accurate state estimation, effectively mitigating the effects of vibration-induced noise in the inertial data. Finally, the framework employs an optimal correspondence selection strategy to identify the most reliable LiDAR point matches, thereby enhancing real-time performance and improving odometry accuracy in dynamic and complex motion scenarios.

Yoshida et al. (2023) proposed a point-cloud mapping technique that employs a helmet-mounted LiDAR sensor for data acquisition by riders using micro-mobility platforms. The method addresses the motion-induced distortion inherent in LiDAR measurements resulting from the rider’s movement and vehicle vibrations. To mitigate this issue, the pose of the helmet—comprising three–dimensional position and attitude angles—-is estimated by integrating information from a Normal Distributions Transform-based Simultaneous Localization and Mapping (NDT-SLAM) algorithm and an Inertial Measurement Unit (IMU). A Kalman filter-based correction algorithm is then applied under the assumption that the helmet exhibits approximately constant translational and angular velocities in any direction. The distortion-corrected LiDAR data are projected onto an elevation map, and measurements corresponding to stationary environmental objects are extracted using an occupancy grid framework. These stationary measurements are subsequently utilized to generate an accurate and consistent point-cloud map of the surrounding environment. While existing approaches have demonstrated improved performance in complex indoor environments, achieving highly precise mapping of as-built structures remains a persistent challenge due to factors such as sensor tilt, occlusions, and irregular floor geometries. To address these limitations, a method has been developed for designed wearable mapping systems (WMSs) that integrates IMU data, LiDAR frames, and RGB imagery within a Simultaneous Localization and Mapping (SLAM) framework to enable accurate 3D point cloud reconstruction of indoor environments.

2. Wearable Mapping System

A wearable scanning platform was developed to enable mobile three-dimensional (3D) perception in constrained or hazardous environments. The developed system is a portable, helmet-mounted data acquisition platform designed for simultaneous 3D scanning and image capture. As illustrated in Figure 1, a LiDAR sensor (Livox MID-360) is integrated with a Rapoo webcam, and both are rigidly mounted on a standard safety helmet to ensure synchronized spatial and visual data collection from the operator’s viewpoint. The system is powered by a compact energy unit consisting of a 12 V, 12 Ah lithium-ion battery, which directly supplies the LiDAR sensor. A high-power 1200 W DC–DC step-up boost converter is employed to regulate and elevate the battery voltage to meet the input requirements of the processing unit. The computational core of the system is an HP G800 mini-PC running Ubuntu 22.04, responsible for sensor interfacing, data logging, and processing. This configuration provides a fully mobile and self-contained solution suitable for field applications requiring 3D mapping and visual documentation.

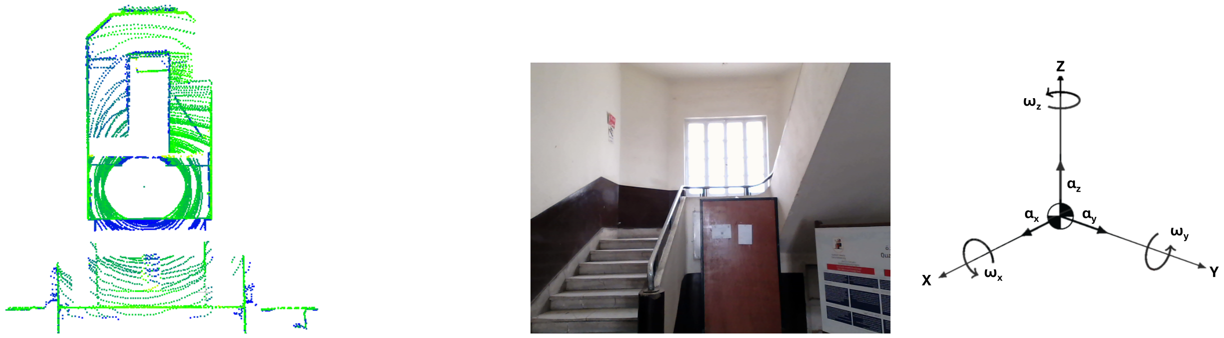

(a) 3D Point cloud (b) RGB image (c) IMU data

Figure 3. Data captured from the proposed system (a): point cloud data (top view), (b): RGB image, and (c): IMU data (accelerometer and gyroscope data)

3. Mapping Methodology

The proposed system collects three different types of data, enabled by the hardware configuration and data collection strategy. These data streams are time-synchronized. The data collection process is designed to adopt the LiDAR sensor as the origin, which serves as the common reference frame for all other sensors (e.g., Camera, IMU). Once the data are collected, the methodology illustrated in Figure 2 is applied. The proposed methodology is divided into three main stages: data collection and system calibration, pose estimation and forward SLAM, and frame registration and map production. Each stage will be discussed in the following subsections.

3.1 Data collection and system calibration

The proposed system comprises a solid-state LiDAR (Livox), an IMU, and an RGB camera. These three sensors are controlled by a mini PC, enabling synchronous data acquisition based on timestamps. The system's acquisition frequency is limited by the lowest sensor rate, which is the LiDAR at 10 Hz, compared to the RGB camera at 30 Hz and the IMU at 200 Hz. At each time instance, the captured point cloud frame, the corresponding RGB image, and IMU data are collected and stored with their respective timestamps. Figure 3 illustrates a sample of the acquired data.

The three sensors have different coordinate systems, which causes a data alignment problem. We use the LiDAR sensor's coordinate system as the common reference. There are two baselines that need calibration: one between the IMU and LiDAR, and another between the RGB camera and LiDAR. Our approach uses IMU data only for gravity correction. Since the baseline between the IMU and LiDAR is small and the rotation between them is considered an identity, we ignore calibration for this baseline.

To calibrate the baseline between the RGB camera and LiDAR, we use an Iterative Closest Point (ICP) method based on surface normals (Chen and Medioni, 1992). This method first employs a deep learning algorithm to generate a point cloud from a sequence of RGB images, then applies ICP to refine the transformation (as shown in Equation 1). Depth Anything 3 (DA3) is used to generate the point cloud from a series of RGB images (Lin et al., 2025).

With known spatial information of both the camera and LiDAR coordinate systems– as the camera's Z-axis is nearly aligned with LiDAR's X-axis, while the camera's Y-axis approximately aligns with LiDAR's Z-axis-– we initialize the rotation between them while assuming zero spatial shift. This initial estimate of rotation and translation helps the ICP algorithm converge quickly to a reliable solution. Additionally, the Perspective-n-Point algorithm (Gao et al., 2003) was applied to a chosen feature point to further enhance the extrinsic camera parameters.

$$\min_{\mathbf{R},,\mathbf{t}} \sum_{i=1}^{N} \left(\mathbf{n}_i^\top \left(\mathbf{R}, \mathbf{p}_i + \mathbf{t} - \mathbf{q}_i \right) \right)^2 \tag{1}$$

where,

$\mathbf{p_i} \in R^3$: point cloud from LiDAR
$\mathbf{q_i} \in R^3$: point cloud from RGB image (DA3)
$\mathbf{n_i} \in R^3$: surface normal at $\mathbf{q}_i$
$\mathbf{R} \in SO(3)$: rotation matrix
$\mathbf{t} \in R^3$: translation vector

3.2 Pose Estimation and Loop Closure Detection

The critical step in the forward SLAM pipeline is the edge pose estimation, which defines the relationship between two successive frames. For this, we adopted the ICP algorithm described in Equation 1, which precisely registers successive LiDAR scans. The initial guess for the relative transformation between frames is estimated from the IMU.Due to small errors between successive frames, after constructing the full pose graph, unavoidable loop closure errors may exist in the graph.

To handle the loop closure issue, we use the g2o graph optimization method to correct both local and global loops, if they exist (Kümmerle et al., 2011). Typically, RGB images are used to detect global loop closures when the drift is large and ICP fails to recognize it. However, in our approach, we rely on ICP for loop closure, considering it a closure if the mapping system returns to a location within 1.4 meters of any previous location. To reduce overlapping poses, we also check frame separation to prevent consecutive loops.

$$\min_{\mathbf{T}_k} \sum (i,j) \in \mathcal{E} \mathbf{e}ij^\top \mathbf{\Omega} ij \mathbf{e}_{ij} \tag{2}$$

where,

$\mathbf{T}_k \in SE(3)$: pose of node k
$\mathcal{E}$: set of edges (constraints)
$\mathbf{e}ij$: error between node i and j
$\mathbf{\Omega}_{ij}$: information (weight) matrix

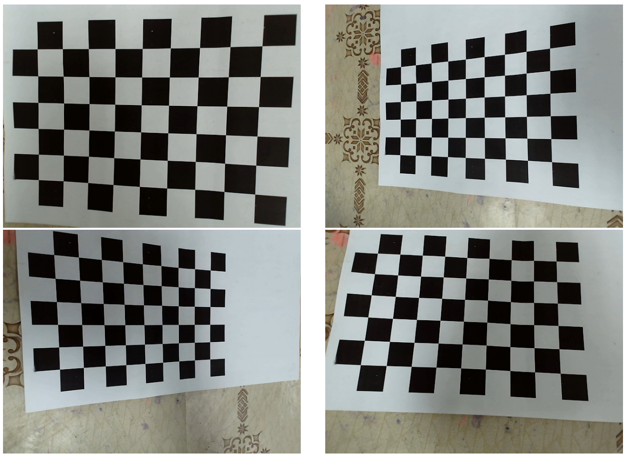

Figure 4. Sample of calibration image

3.3 Frame Registration and global map production

After detecting and correcting the loop closure, the global trajectory is updated based on the g2o algorithm. Since, for each frame, we have the optimized pose data. The global map was constructed using Equation 3. There is no additional transformation needed at this stage, as the calibration assumes that the system global frame coincides with the LiDAR sensor.

$$\mathcal{M} = \bigcup_{k=1}^{N} \left\{ \mathbf{R}_k \mathbf{p}_k^i + \mathbf{t}_k \right\} \tag{3}$$

where,
$\mathbf{p}_k^i$ is the i-th point in frame k,
$\mathbf{R}_k$ and $\mathbf{t}_k$ are the rotation and translation of frame k in the global coordinate system,
N is the total number of frames.

4. Experiments and Discussion

The baseline between the RGB camera and LiDAR (camera extrinsics) is computed using a point cloud registration method and the traditional PnP algorithm. As it is advantageous to supply the camera's intrinsic parameters to the DA3 pipeline when feeding data into the algorithm, the Zhang calibration method (Zhang, 2000) was applied to estimate the camera intrinsics with 37 captured images. Figure 4 shows a sample of the images used for intrinsic calibration. Table 1 presents the camera calibration results, including both intrinsic and extrinsic parameters. It is worth noting that the mean re-projection error of the calibration pipeline is 0.393 pixels.

Intrinsic parameters (pixels)			
f_x	f_y	C_x	C_y
445.23	445.91	319.38	255.28
Distortion parameters (dimensionless)			
K_1	K_2	p_1	p_2
0.13698	-0.2034	0.0055	0.0019
Extrinsic parameters (meters–degrees)			
t_x	0.171	θ_x	-86.4573046
t_y	-0.019	θ_y	0.48190462
t_z	-0.023	θ_z	-88.94943855

Table 1. Camera calibration parameters: Euler angles are represented in degrees.

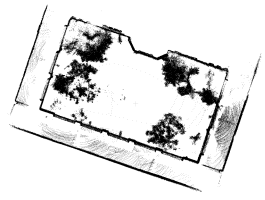

(a) Courtyard

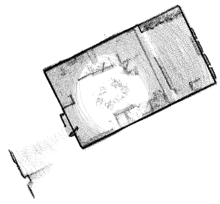

(b) Room

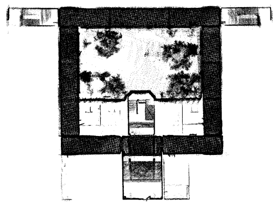

(c) Hallway

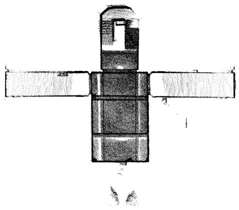

(d) Entrance

Figure 5. Captured dataset

To evaluate the proposed method, four experiments were conducted with trajectories ranging from 4 meters to 100 meters. Table 2 summarizes these experiments. The data were processed under two different pose estimation conditions: the first employed a pure ICP point-to-plane algorithm with the identity matrix as the initial transformation, while the second incorporated IMU data to estimate the relative roll and pitch angles, which were used as the initial guess for ICP, as depicted in Figure 2 through gravity alignment.

Figure 5 shows the point clouds produced by the proposed methodology for the four different experiments. The dataset covers a range of depths captured by the Livox sensors, starting from 2.0 meters (in the Room dataset) up to 25 meters (in the Hallway dataset). Additionally, the experiments encompass different types of environments: indoor environments (Room and Entrance), narrow spaces (Hallway), and outdoor environments (Courtyard). These experiments provide a comprehensive evaluation of the proposed methodology. To assess the quality of the resulting point cloud, a statistical analysis of the wall surfaces was conducted. The metrics used to evaluate point cloud quality are based on the distribution of points around the wall surfaces. To achieve this, the global point cloud was aligned with gravity and then projected onto the XY plane. The resulting 2D point cloud was used to extract wall points. RANSAC-based line fitting was applied to detect the walls, and a buffer of 100 mm was defined around each fitted line to evaluate the registration quality using the mean, median, and standard deviation. Figure 6 illustrates the projected density of the point cloud for both ICP and ICP + IMU-based modes. Table 3 presents the statistical measures for the four experiments.

It can be seen from Table 3 that the ICP + IMU mode noticeably improves the overall quality of the final point cloud, especially for the median, which completely reflects the outliers from re-

Experiment	Hallway	Room	Entrance	Courtyard
Trajectory Length (m)	89.80	4.39	20.3	36.90
Key Frames (counts))	171	53	106	79
Mapped Area (m^2)	625	33	117	405

Table 2. Experiment's statistics and description: Trajectory length computed based on minimum loop-closing error.

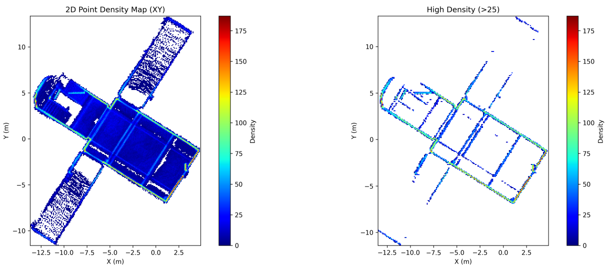

(a) ICP reuslts

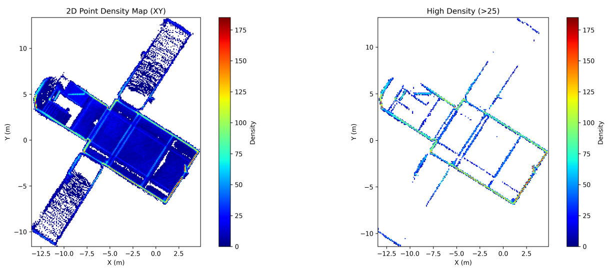

(b) ICP + IMU results

Figure 6. Projected point to XY plan for Entrance dataset.

Experiment	Hallway		Entrance	
Odometry	ICP+IMU	ICP	ICP+IMU	ICP
Mean	33.78	43.95	37.37	37.94
Median	27.72	41.1	33.23	33.67
std	25.93	28.28	25.64	26.33
Experiment	Room		Courtyard	
Odometry	ICP+IMU	ICP	ICP+IMU	ICP
Mean	29.78	45.05	36.28	38.92
Median	25.05	42.76	31.17	34.15
std	22.25	28.03	26.2	26.87

Table 3. Quality indicators for the registered point cloud (units are in mm).

gistration. Also, it can be noted that the standard deviation is almost the same; it is around 26 mm. This reflects that the noise produced from the sensor itself is around 26 mm regardless of odometry mode. Taking into consideration the sensor noise, the proposed method can reconstruct the floor maps to a 3-mm level of precision using the ICP + IMU fusion, while it reaches a 12-mm level of precision using ICP mode. This can be clearly observed from Figure 6, as the density maps appear visually indistinguishable and therefore confirm the accuracy levels stated in Table 3.

To verify the absolute accuracy of the generated point cloud, fifteen measurements were collected from the mapped areas, and the corresponding distances were measured from the produced point cloud (using ICP+IMU mode). As shown in Table 4, the results demonstrated that the mean error is -5 mm and the standard deviation is 26 mm. This reflects that the proposed approach does not add additional error due to registration, and the resulting model has only the sensor noise and a perfect registration.

D	Ground truth	Measured	Error	Absolute Error(%)
1	4.26	4.25	0.01	0.24
2	7.47	7.47	0.00	0.00
3	4.30	4.29	0.01	0.23
4	2.91	2.93	-0.02	0.68
5	2.93	2.95	-0.02	0.68
6	2.40	2.41	-0.01	0.41
7	2.95	2.93	0.02	0.68
8	3.07	3.13	-0.06	1.92
11	6.67	6.72	-0.05	0.74
12	8.09	8.07	0.02	0.25
13	8.00	7.97	0.03	0.38
14	6.70	6.71	-0.01	0.15
15	4.44	4.43	0.01	0.23
Mean	-	-	-0.005	0.507
Std	-	-	0.026	0.467

Table 4. Ground truth distances (D) versus the measured distances from point cloud; units are in meters.

5. Conclusions

In this research, we present a mapping system based on a Livox LiDAR sensor integrated with an RGB camera. The system is designed to generate floor maps; however, all computations and processing are performed in 3D space. The system calibration includes intrinsic calibration of the RGB camera and extrinsic calibration between the RGB camera and the LiDAR. A novel calibration method that integrates Depth Anything 3 with the PnP algorithm is proposed to effectively estimate the extrinsic parameters of the RGB camera. A SLAM-based point cloud registration framework is developed using two odometry modes: a plane-based ICP approach and an ICP + IMU-based approach. The overall performance of the proposed method achieves a relative precision of approximately 3 mm using the ICP + IMU mode, compared to about 12 mm when using ICP alone, and achieves absolute accuracy of 26 mm.

6. Acknowledgments

The authors gratefully acknowledge Ahmed Saad, affiliated with NAMAA Consult Company, for his valuable contributions to this research through the deployment of the DA3 algorithm.

References

Chen, Y., Medioni, G., 1992. Object modelling by registration of multiple range images. *Image and vision computing*, 10(3), 145–155.

Gao, X.-S., Hou, X.-R., Tang, J., Cheng, H.-F., 2003. Complete solution classification for the perspective-three-point problem. *IEEE transactions on pattern analysis and machine intelligence*, 25(8), 930–943.

Hany, Y., Ahmed, W., Elshazly, A., Senousi, A. M., Darwish, W., 2025. Automated 3D Reconstruction of Interior Structures from Unstructured Point Clouds. *ISPRS International Journal of Geo-Information*, 14(11). https://www.mdpi.com/2220-9964/14/11/428.

Kümmerle, R., Grisetti, G., Strasdat, H., Konolige, K., Burgard, W., 2011. G2o: A general framework for graph optimization. *2011 IEEE International Conference on Robotics and Automation*, 3607–3613.

Li, J., Yuan, S., Cao, M., Nguyen, T.-M., Cao, K., Xie, L., 2024. HCTO: Optimality-aware LiDAR inertial odometry with hybrid continuous time optimization for compact wearable mapping system. *ISPRS Journal of Photogrammetry and Remote Sensing*, 211, 228-243.

Lin, H., Chen, S., Liew, J., Chen, D. Y., Li, Z., Shi, G., Feng, J., Kang, B., 2025. Depth anything 3: Recovering the visual space from any views. *arXiv preprint arXiv:2511.10647*.

Mahmoud, M., LI, Y., Adham, M., CHEN, W., 2025. Automated material-aware BIM generation using deep learning for comprehensive indoor element reconstruction. *Automation in Construction*, 175, 106196.

Sánchez-Aparicio, L. J., Del Pozo, S., Ramos, L. F., Arce, A., Fernandes, F. M., 2018. Heritage site preservation with combined radiometric and geometric analysis of TLS data. *Automation in Construction*, 85, 24-39.

Wang, H., Li, M., 2024. A New Era of Indoor Scene Reconstruction: A Survey. *IEEE Access*, 12, 110160-110192.

Wang, S., Li, H., Miao, T., Gao, Z., Song, A., 2025. Feature Extraction of Horizontal Plane and Optimization of 3-D LiDAR SLAM in Indoor Environments. *IEEE Transactions on Instrumentation and Measurement*, 74, 1-18.

Willkens, D. S., Liu, J., Alathamneh, S., 2024. A Case Study of Integrating Terrestrial Laser Scanning (TLS) and Building Information Modeling (BIM) in Heritage Bridge Documentation: The Edmund Pettus Bridge. *Buildings*, 14(7). https://www.mdpi.com/2075-5309/14/7/1940.

Wu, H., Liu, Y., Wang, C., Wei, Y., 2025. An Effective 3D Instance Map Reconstruction Method Based on RGBD Images for Indoor Scene. *Remote Sensing*, 17(1). https://www.mdpi.com/2072-4292/17/1/139.

Xu, Z., Fischer, S., Holst, C., 2025. Uncertainty-aware Evaluation and Fusion of Point Clouds for Simultaneous Scanning of Two State-of-the-art Indoor MLS Systems. *The International Archives of the Photogrammetry, Remote Sensing and Spatial Information Sciences*, XLVIII-G-2025, 1603–1610. https://isprs-archives.copernicus.org/articles/XLVIII-G-2025/1603/2025/.

Yoshida, I., Yoshida, A., Hashimoto, M., Takahashi, K., 2023. Map building using helmet-mounted LiDAR for micromobility. *Artificial Life and Robotics*, 28(2), 471–482.

Zhang, D., Tan, W., Zelek, J., Ma, L., Li, J., 2025. SLAM-TSM: Enhanced Indoor LiDAR SLAM With Total Station Measurements for Accurate Trajectory Estimation. *IEEE Transactions on Intelligent Transportation Systems*, 26(2), 1743-1753.

Zhang, Z., 2000. A flexible new technique for camera calibration. *IEEE Transactions on pattern analysis and machine intelligence*, 22(11), 1330–1334.

Zhao, Y.-L., Hong, Y.-T., Huang, H.-P., 2024. Comprehensive Performance Evaluation between Visual SLAM and LiDAR SLAM for Mobile Robots: Theories and Experiments. *Applied Sciences*, 14(9). https://www.mdpi.com/2076-3417/14/9/3945.